Synthesis of Fe_3O_4/ ZnO/CuO Nanocomposite and its Sono-photocatalyst property for removal of methylene blue from wastewater

Samira Pishkar Ahrab[1], Mahdiyeh pourali[2], MohammadTaghi Hamedani[*1],

1. Faculty of Mechanical Engineering, Tabriz University, Tabriz, 51616471, Iran.
2. Faculty of Materials Engineering, Sahand University of Technology, Tabriz, 513351996, Iran.

Abstract

Fe_3O_4/ZnO/CuO nanocomposites with various molar ratios of CuO were successfully synthesized. Sol-gel method was used to syntehesize nanocomposite materials at a low temperature. A set of experiments, including X-ray diffraction (XRD), Dynamic Light Scattering (DLS),) scanning electron microscopy (SEM), and UV-Vis spectroscopy, was used to confirm the successful synthesis of Fe_3O_4/ZnO/CuO nanocomposites in crystalline form.

The photocatalytic activity of the samples was investigated via the degradation of methylene blue (MB) dye from synthetic wastewater under three distinct conditions: visible light, ultraviolet light, and a combination of visible light with ultrasonic treatment. Fe_3O_4/ZnO/CuO nanocomposite with a molar ratio of 1:1:0.5 showed the highest photocatalytic activity when irradiated with either visible or ultraviolet light. Furthermore, when visible light was combined with ultrasonic treatment, complete (100%) removal of methylene blue was achieved within 120 minutes. The results demonstrate that these nanocomposites are efficient catalysts for wastewater treatment through the removal of organic pollutants.

Keywords Fe_3O_4/ZnO/CuO, Sono-photocatalyst, nanocomposite, Wastewater treatment

1 Introduction

Over the past few decades, there have been some emerging problems in the industry, whereas environmental pollution has attracted a lot of attention in the world [1]. The release of organic dyes from the textile, leather, food, cosmetics, and pharmaceutical industries into the environment has resulted in significant issues for living organisms. Also, water pollution is a problem that should be identified as soon as possible. Researchers have done a great deal of research on how to treat infected water from the processing of industrial products and household waste [2]. Nevertheless, the conventional wastewater treatment method still contains a large number of contaminants that are challenging to eliminate. For instance, antibiotics, dyes, organic insecticides, multi-rheological aromatic hydrocarbons [3-6], etc. New techniques, like Fenton oxidation [7] and a hybrid approach that combines multiple purification processes, like active carbon, biofilm, enzymatic reactors, etc., have been developed to remove these contaminants [8]. These techniques have garnered interest from researchers [9] and have a positive impact on the degradation of contaminated organic matter. Another method for removing

[*] Corresponding author
Professor of Materials science and engineering, Mechanic faculty, Tabriz university, Tabriz ,Iran.
Email m.hamedani.tabrizu@gmail.com, Tel: +989147618082 & +98-41-33356026, Fax: +98-41-33354153

[DOI: 10.22068/ijmse.4019]

pollutants is to use Semiconducting oxides with photocatalytic properties. Various catalysts have been introduced to remove pollutants or even make them non-irritating chemicals [10]. Among them, TiO_2 and ZnO semiconductors have been introduced as successful photocatalysts for the destruction of organic pollutants. The advantages of ZnO nanoparticles include strong oxidizing ability, light sensitivity, excellent mechanical and chemical stability, non-toxic nature, favorable energy gap, and cheap price [11]. However, to use ZnO as a photocatalyst, according to the band gap (3.2 electron volts), it is necessary to use ultraviolet light that only contains less than 10% of the sun's light. While in the sunlight, 45% of the radiation is visible in the light range [12,13]. To enhance the photocatalytic activity of ZnO under the influence of visible light, solutions need to be considered. The formation of a ZnO nanoparticle composite with other metal oxides results in the absorption of stronger light and increased ability to absorb visible light [14]. In addition, this composite prevents recombining electron-hole and increases the photocatalyst's efficiency [15]. The coupling of ZnO with CuO nanoparticles and their composite formation is a promising method for increasing photocatalytic properties. Besides extending the absorption range towards the visible light, this method transmits electrons produced by the photon from a high-conductivity band of CuO to a low-conductvity band of ZnO, which results in the effective separation of the electron-hole [16]. So far, considerable research has been done on the synthesis of ZnO / CuO as a special high-level catalyst. Number of techniques have been put up to create a ZnO/CuO catalyst, such as mechanical methods, for example grinding, wet chemistry, coprecipitation, thermal decomposition, sol-gel, hydrothermal, and photo deposition methods [17]. Another problem for catalysts is their segregation from purified water in practical applications. Traditional methods such as coagulation and filtration cause catalyst degradation and increase energy consumption [18]. Using an external magnet, researchers have recently paired magnetic nanoparticles with photocatalytically active materials to improve catalyst separation and recycling [19].

Therefore, the introduction of magnetic materials such as Fe_3O_4 in Fe_3O_4/ZnO/CuO nanocomposites simplifies the magnetic separation. Nanocatalysts are beneficial for academic and industrial research due to their high reaction rates, perfect activation of adsorbed compounds, ease of use, high selectivity, recyclability, and eco-friendliness. Because of their appealing features, nanometal oxides have been utilized as solid catalysts in a variety of organic processes [20].

In explaining the photocatalytic effect, it can be said that in the absence of degradation matter, hydrocarbons often decompose slowly. Photocatalyst reduces the activation energy of the decomposition process and therefore, accelerates the reaction. As a result of the light collision with photocatalytic materials, electron holes create high oxidation and resuscitation [21].

Nowadays, the use of ultrasonics in the presence of a catalyst (sonocatalytic decomposition) is an eco-friendly method for removing dyes from wastewater. The influence of ultrasonic waves is the heat produced by a hole explosion, which converts water molecules into hydroxyl radicals and reactive hydrogen atoms. Both species can react with organic dyes, which can lead to the breakdown and elimination of different contaminants from wastewater[22].

As a result, the simultaneous use of light and ultrasonic radiation to analyze different colors has been investigated [19-22].

In the current study, the impact of light and ultrasound irradiation and the metal oxide content has been investigated on the photocatalytic activity of the Fe_3O_4/ZnO/CuO nanocomposites. The optical and morphological analysis proceeded with a photocatalytic activity test in methylene blue (MB) degradation from wastewater.

2 EXPERIMENTAL PROCEDURES

In this study Iron (II) sulfate heptahydrate ($FeSO_4 \cdot 7H_2O$, 99%), copper sulfate pentahydrate ($CuSO_4 \cdot 5H_2O$, 99%), zinc sulfate

[DOI: 10.22068/ijmse.4019]

heptahydrate ($ZnSO_4 \cdot 7H_2O$, 99%) and sodium hydroxide (NaOH) (Merck Company) was used as raw materials.

CuO and Fe_3O_4 nanoparticles were synthesized using the sol-gel method. In this method, 0.025 mole of $CuSO_4 \cdot 5H_2O$ was dissolved in 100 mL of deionized water with constant magnetic stirring. Then 0.05 mole of NaOH was dissolved in 150 mL of deionized water and added to the solution in a droplet form to obtain the appropriate pH. The solution was then maintained at 80 ° C for 3 hours to form the gel. After 4 hours, the black product was dissolved using filter paper and dried at 80 ° C for 4 hours in an oven to achieve Copper oxide nanoparticles.

To obtain Fe_3O_4 nanoparticles, 0.027 mole of $FeSO_4 \cdot 7H_2O$, dissolved in 100 mL of deionized water and continuously stirred at room temperature. To control the pH in 3, acetic acid (CH_3COOH) and 30 mL of ethylene glycol (EG), both of them in pure form, were added to the solution. Then, 0.054 mole of NaOH was dissolved in 150 mL of deionized water and added dropwise to the mixture. The final solution was stirred at 80 °C for 3 h to form a gel. The gel was dried at 80 °C for 4 h.

To synthesize the Fe_3O_4/ZnO/CuO nanocomposite, 0.0125 mole of $ZnSO_4 \cdot 7H_2O$ was dissolved in 30 mL of distilled water with magnetic stirring. Then, 0.025 mole of NaOH in 65 mL of deionized water was added to the solution in droplets to reach the appropriate PH, which was then stirred and heated at 80 °C. The previously synthesized Fe_3O_4 and CuO nanoparticles were dispersed in 30 mL of ethanol(99.7%) and then added to the initial solution. The resulting mixture was continuously stirred at 80 °C for 2 hours. Finally, ZnO was formed in situ on the surface of the pre-formed Fe_3O_4 and CuO. At the end the product was isolated using filter paper and washed several times with distilled water and ethanol to remove impurities. The final product was left at room temperature overnight and dried at 100 ° C for 1 hour. Nanocomposite Fe_3O_4/ZnO/CuO with the molar ratios of (1:1:0.3, 1:1:0.5, 1:1:1, 1:1:3) was prepared by changing the concentrations of the precursor solutions and evaluated.

X-ray diffraction peaks were measured by an XRD analyzer (Siemens D5000 X-ray diffractometer). The analysis was conducted under the conditions of Cu-kα radiation (λ=1.54178Å), a scanning rate of 20º/min, a 2θ range of 20–80º, and operating conditions of 30 kV and 40 mA. Also, Crystallite size is estimated by Scherer's equation (Eq.1) [23]:

$$D=0.9\lambda/\beta Cos\Theta \quad \text{(Eq. 1)}$$

where D is the size of the crystals in nanometers, ß is the peak width at half the maximum intensity in radians in radian, λ is the x-ray wavelength in nanometers, and Θ is the Bragg angle corresponding to the diffraction peak.

SEM (Stereo Scan 360) was conducted to verify the morphology of the obtained nanoparticles. Elemental analysis of the samples was performed using X-ray diffraction spectroscopy (EDX). A dot map was used to determine the distribution of the elements in the nanocomposite. To investigate particle size distribution from DLS, Nanotrac Wave of Micro trac Co. was used and to determine the adsorption edge and band gap of synthesized zinc oxide and prepared nanocomposites, DRS spectroscopic analysis was performed. The absorption wavelength was obtained by extrapolating the linear part of the absorption intensity curve in terms of wavelength.

Eq. 2 was used to calculate the band gap [24]:

$$Eg = hc / \lambda g \quad \text{(Eq. 2)}$$

In this respect, Eg is the band gap in electron volts, h is the Planck constant equals 4.13567×10^{-15} ev, c is the light speed equals 299792458 m / s and λg is the absorption wavelength.

The effectiveness of the photocatalysts was tested by measuring their ability to break down methylene blue (MB) in 100 mL beakers. In this test, the UV-C Philips 9W lamp was used as UV light and the 120-watt metal halide lamp was used as a visible light source. A photocatalytic test equipment was mounted and sealed in a dark chamber to prevent the loss of radiation. For the determination of photocatalytic activity, 0.05 g of the nanocomposite samples was dispersed in 100 ml of MB solution with a concentration of 0.005 g / l using a magnetic stirrer. Before illumination, the reaction mixture was

[DOI: 10.22068/ijmse.4019]

kept in dark conditions for 20 minutes to establish adsorption-desorption equilibrium. After collecting the initial sample, the photocatalytic reaction was initiated by activating the light source. Subsequent samples were collected at 20-minute intervals (specifically at 20, 40, 60, 80, 100, and 120 minutes), and each sample underwent UV-Vis spectroscopic analysis. The concentration of Methylene Blue (MB) was determined by measuring the UV-Vis absorbance at its characteristic peak wavelength of 665 nm. A calibration curve was created and used to convert the measured absorbance values into actual dye concentrations. The degradation rate was then determined using the following equation [25]:

$$(I_0-I_t)/I_0 \times 100 = (C_0- C_t)/C_0 \times 100 \qquad \text{(Eq. 3)}$$

Where C represents the concentration of Methylene Blue (MB) at any given time during the reaction, while C0 is the initial MB concentration after reaching adsorption-desorption equilibrium, similarly, A represents the absorbance value measured at any point during the reaction, and A0 is the initial absorbance value recorded at equilibrium. To evaluate how ultrasonic treatment affects photocatalytic activity, Fe_3O_4/ZnO/CuO nanocomposites (0.05 g) with varying molar ratios were dispersed in Methylene Blue solution (100 mL, 0.005 g/L) using ultrasonication and subjected to visible light irradiation for intervals of 20, 40, 60, 80, 100 and 120 minutes.

3 Results and Discussions

The XRD patterns shown in Fig. 1 display the diffraction patterns of Fe_3O_4/ZnO/CuO nanocomposites that were synthesized in different molar ratios of CuO. The patterns exhibit characteristic diffraction peaks corresponding to cubic spinel Fe_3O_4, monoclinic CuO, and hexagonal wurtzite ZnO structures. The absence of any impurities or secondary phases in the patterns demonstrates that the Fe_3O_4/ZnO/CuO nanocomposites were synthesized successfully. All XRD peaks corresponding to [101] Planes related to hexagonal ZnO structure (2Θ =32.5), [200] planes related to CuO monoclinic structure (2Θ =39.5) and [311] planes for cubic spinel structure Fe_3O_4 (2Θ =35.5) have the highest growth rates. Furthermore, analysis of the XRD patterns for Fe_3O_4/ZnO/CuO nanocomposites with varying molar ratios reveals a clear trend: as the molar ratio of CuO to ZnO increases, there is a corresponding increase in the intensity of CuO diffraction peaks, while simultaneously showing a decrease in the intensity of both ZnO and Fe_3O_4 diffraction peaks. Changes in the intensity of the pattern revealed the increase of CuO content within the nanocomposite structure.

In all XRD diagrams, considering the peak positions, it can be seen that ZnO does not form a solid solution with CuO and Fe_3O_4, and the Fe_3O_4/ZnO/CuO nanocomposite is considered as a nanocomposite powder of ZnO, Fe_3O_4 and CuO crystals.

Fig. 2 shows the XRD pattern of Fe_3O_4/ZnO/CuO nanocomposite with molar ratios of 1:1:0.3, 1:1:0.5, 1:1:1, and 1:1:3 for a,b,c, and d images, respectively. According to reference data, 01-075-0033 demonstrated Fe_3O_4 in the cubic phase, 0254-041-00 determined the hexagonal crystalline phase of ZnO, and 0704-076-01 demonstrated CuO with a monoclinic crystalline structure.

In Table. 1, the particle size of Fe_3O_4, ZnO, CuO, and Fe_3O_4/ZnO/CuO nanocomposites with molar ratios of 1:1:0.3, 1:1:0.5, 1: 1: 1 and 1: 1: 3 estimated by Scherrer's equation. By comparing the size of Fe_3O_4, ZnO, and CuO particles in Fe_3O_4/ZnO/CuO nanocomposites with different molar ratios, it is observed that the presence of CuO inhibits the growth of particles and reduces the size of ZnO and Fe_3O_4 particles.In conclusion, CuO nanoparticles inhibit the growth of ZnO crystallites. It was evidenced by the significant reduction in ZnO crystallite size in the presence of CuO. In contrast, Fe_3O_4 crystallite size shows a smaller

[DOI: 10.22068/ijmse.4019]

decrease, indicating that CuO has a less pronounced effect on the growth of Fe_3O_4 crystallites. The crystallite size of CuO varies depending on its concentration in the composites, highlighting its role in controlling crystallite growth in nanocomposites.

Table1. crystallite size of ZnO, CuO, and Fe_3O_4 in Fe_3O_4/ZnO/CuO nanocomposite

samples	ZnO crystallite size (nm)	CuO crystallite size (nm)	Fe_3O_4 crystallite size (nm)
Fe_3O_4	-	-	44.5
CuO	-	19.31	-
ZnO	22.92	-	-
Fe_3O_4/ZnO/CuO(1:1:0.3)	19.21	20.15	44.01
Fe_3O_4/ZnO/CuO (1:1:0.5)	20.18	16.15	42.23
Fe_3O_4/ZnO/CuO (1:1:1)	19.65	18.62	41.15
Fe_3O_4/ZnO/CuO (1:1:3)	17.15	21.48	40.15

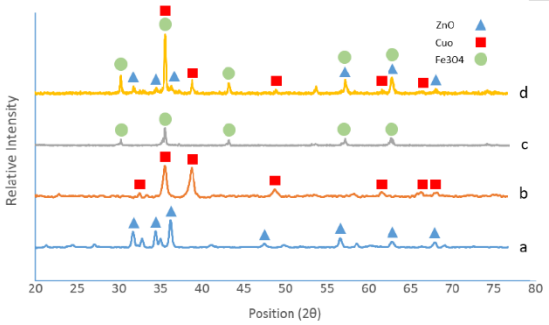

Fig. 1. XRD patterns of synthesized Fe_3O_4/ZnO/CuO nanocomposite: (a) ZnO, (b) CuO, (c) Fe_3O_4, (d) Fe_3O_4/ZnO/CuO nanocomposite.

Particle morphology of nanocomposites was investigated by scanning electron microscopy (SEM). Fig. 3 illustrates an SEM image of a Fe_3O_4/ZnO/CuO nanocomposite with a molar ratio of 1:1:0.5. As shown in Fig.3, the Fe_3O_4/ZnO/CuO nanocomposite is cauliflower-shaped. To compare the results, the size distribution of the conventional and synthesized catalysts was considered using ImageJ software. The analysis revealed that the synthesized samples exhibited relatively small average particle dimensions. This size distribution indicates the successful formation of nanostructured materials. Similar Fe_3O_4/ZnO/CuO morphologies have been reported in previous studies[20].

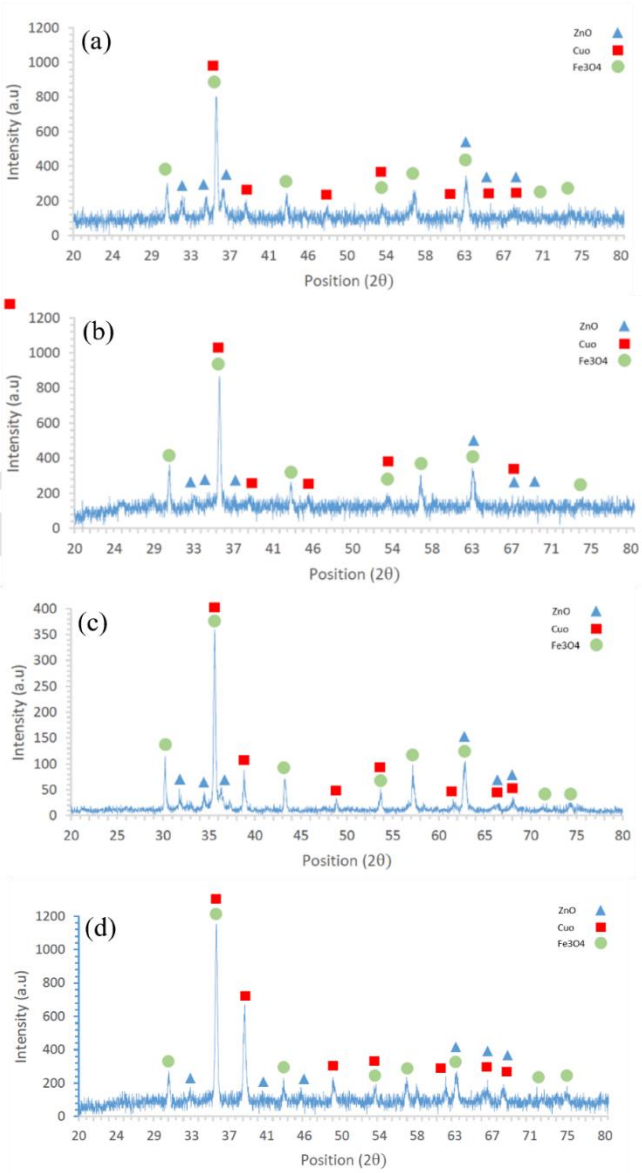

Fig. 2. XRD patterns of synthesized Fe_3O_4/ZnO/CuO nanocomposite: (a) Fe_3O_4/ZnO/CuO (1:1:0.3), (b) Fe_3O_4/ZnO/CuO(1:1:0.5), (c) Fe_3O_4/ZnO/CuO (1:1:1) and (d) Fe_3O_4/ZnO/CuO(1:1:3).

Above all, the numerous pores of different sizes within the 3D microstructure act as transport pathways for small molecules. This morphology and porosity provide a larger surface area for dye adsorption and catalytic reactions. The reduction in particle dimensions

[DOI: 10.22068/ijmse.4019]

enhances the generation of electron-hole pairs when exposed to light, resulting in more effective degradation of contaminants during performance testing.

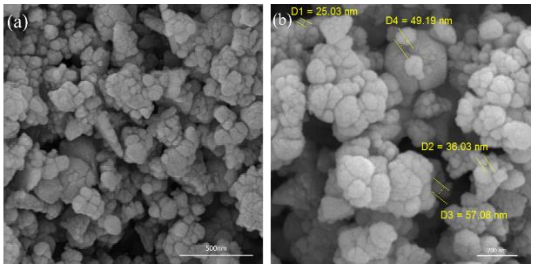

Fig. 3. SEM image of synthesized Fe_3O_4/ZnO/CuO nanocomposite, (a)SEM Mag 70kx (b) SEM Mag 100kx Particle Size Distribution

EDX analysis aims to define the dispersion of the elements on the surface of the catalyst. As shown in Fig. 4, the characteristic peaks of the elements of oxygen, iron, copper, and zinc indicate the presence of these elements in the nanocomposite structure. It should be noted that the samples had no impurities. The peak in the range of 1.8 and 2.2 keV is related to the gold element, covered on the nanocomposite in SEM analysis, to provide conductivity in the sample. Also in Table 2, the weight percentage and atomic percentage of the elements are specified, which proves the proper synthesis of the samples.

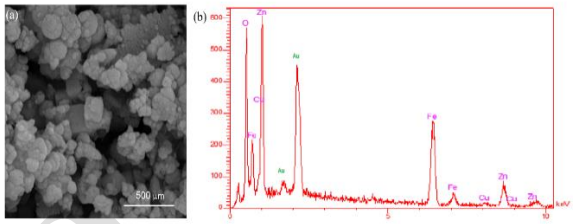

Fig. 4. EDX analysis of synthesized Fe_3O_4/ZnO/CuO nanocomposite: (a) SEM image of the area selected for EDX analysis, (b) EDX results in Fe_3O_4/ZnO/CuO nanocomposite (1:1:0.5)

Table 2. Comparative amount of elements in the structure of Fe_3O_4/ZnO/CuO nanocomposite (1:1:0.5)

samples	Weight percentage (% W)	Atomic percentage (% A)
$O_{K\alpha}$	28.77	60.03
$Cu_{K\alpha}$	1.72	0.9
$Zn_{K\alpha}$	28.38	14.49
$Fe_{K\alpha}$	41.12	24.57

To investigate the distribution of elements in the photocatalyst structure, dot Map analysis was prepared from Fe_3O_4/ZnO/CuO nanocomposite (1:1:0.5) as shown in Fig. 5. The elemental distribution analysis of the photocatalyst structure was conducted on the selected region shown in Fig. 5a. Images 5b, 5c, 5d, and 5e show the distribution of copper, iron, zinc, and oxygen, respectively. Moreover, the elements are homogeneously distributed in the structure.

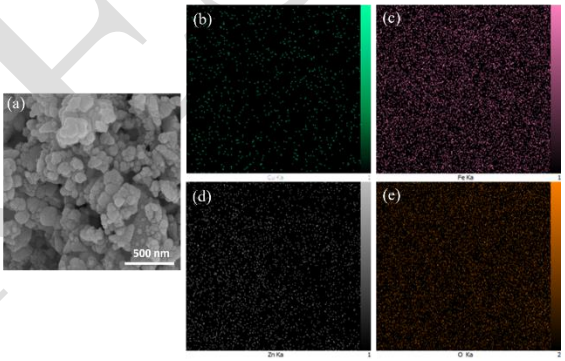

Fig. 5. Dot map analysis of synthesized Fe_3O_4/ZnO/CuO nanocomposite: (a) Selected area for dot map analysis, (b) Cu, (c) Fe, (d) Zn, (e) O

In this study, the photocatalytic performance of Fe_3O_4/ZnO/CuO nanocomposites was investigated by analyzing the relationship between band gap and varying molar ratios of the components. The photocatalytic degradation efficiency of pollutants is primarily determined by the band gap, which serves as the critical parameter in the process. For this purpose, the absorption spectrum of nanocomposites was measured by a UV-visible device, and the results are shown in Fig. 6(a). The bandgap energies of the samples were determined using Tauc's plots by extrapolating the linear part of plots to the hν axis as shown in Fig.6 (b).

ZnO nanoparticles exhibit strong absorption in the wavelength range of 200-400 nm, and the

[DOI: 10.22068/ijmse.4019]

absorption edge of the samples shifts to 372 nm with increasing copper oxide content in the visible light region. Coupling zinc oxide with copper oxide leads to a narrowing of the band gap. This reduction in the band gap occurs because the addition of copper oxide to the nanocomposite introduces an intermediate energy band at the bottom of the conduction band of zinc oxide. This interaction decreases the energy difference between the valence band and the conduction band of zinc oxide, thereby reducing the overall band gap energy.

According to the literature, ZnO nanoparticles are n-type semiconductors, and the semiconductor CuO nanoparticles are p-type. In this study, the photocatalytic performance was enhanced by creating a heterojunction between n-type and p-type semiconductors, while simultaneously studying how this junction influences the optical characteristics. In Table 3, the absorption wavelength and energy of the band gap region for each sample are calculated using the following equation:

$$(\alpha h\nu)^2 = A(h\nu - Eg) \quad \text{(Eq.4)}$$

where α is the absorption coefficient, h is Planck's constant, v is the photon frequency, Eg is the optical band gap, and A and n are constants. For the direct bandgap semiconductor, n = 2, and for the indirect transition bandgap, n=½. We assumed n = 2 for our samples.

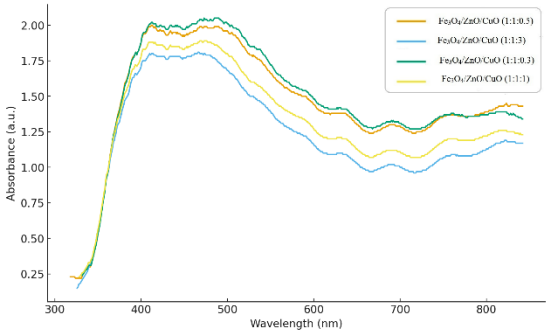

a)

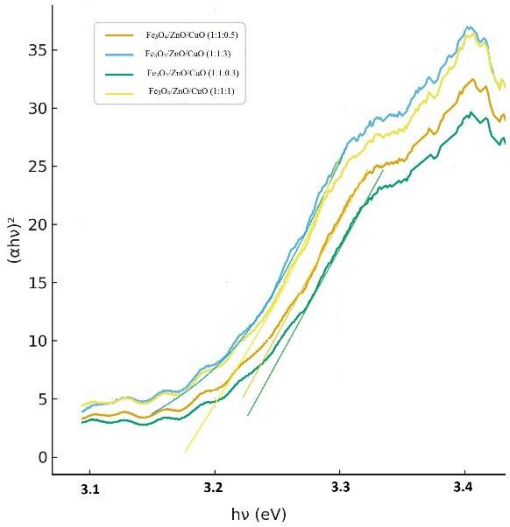

b)

Fig. 6 . Bandgap analysis curves of Fe_3O_4/ZnO/CuO nanocomposite: a) UV-VIS Absorption Spectra, b) Tauc's plots graphs (n=2)

Table 3. Wavelength values of the absorption edge and the energy of the band gap of ZnO and Fe_3O_4/ZnO/CuO nanocomposites

Samples	Wavelength of absorption edge (nm)	Energy of the band gap (eV)
ZnO	382.16	3.24
Fe_3O_4/ ZnO/ CuO (1:1:0.3)	384.1	3.22
Fe_3O_4/ ZnO/ CuO (1:1:0.5)	386.31	3.20
Fe_3O_4/ ZnO/ CuO (1:1:1)	389.26	3.18
Fe_3O_4/ ZnO/ CuO (1:1:3)	398.54	3.11

DLS analysis was performed to investigate particle size distribution. Fig. 7 illustrates the range of particle size distribution in the ZnO, Fe_3O_4/ZnO/CuO(1:1:0.3), Fe_3O_4/ZnO/CuO(1:1:0.5), Fe_3O_4/ZnO/CuO(1:1:1)and Fe_3O_4/ZnO/CuO(1:1:3) samples are 486-1944, 486-6540, 25-409,289-6540, 171.9-6540 nm, respectively.

On the other hand, the highest number of particles in the ZnO, Fe_3O_4/ZnO/CuO(1:1:0.3), Fe_3O_4/ZnO/CuO (1:1:0.5), Fe_3O_4/ZnO/CuO (1:1:1), and Fe_3O_4/ZnO/CuO (1:1:3) samples are 972, 687, 30.04, 289, and 171.9 nm, respectively. DLS measures the hydrodynamic diameter of particles (or agglomerates) in a solution, which is typically much larger than

[DOI: 10.22068/ijmse.4019]

the primary particle size seen in SEM or the crystallite size from XRD. The results show that increasing the percentages of CuO in the Fe_3O_4/ZnO/CuO nanocomposite does not have a steady effect on particle size. In general, although the particle size in the nanocomposite decreased compared to the particle size in pure ZnO samples but also the DLS data also indicate severe agglomeration of the primary nanoparticles in suspension, which is a critical factor for photocatalytic performance as it affects the active surface area.

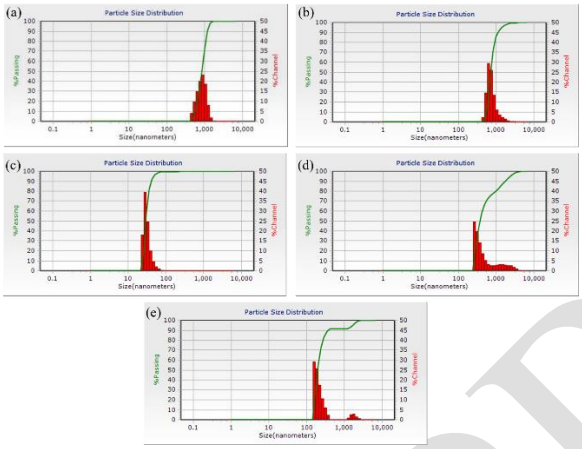

Fig. 7. DLS Analysis Results of Fe_3O_4/ZnO/CuO nanocomposites, (a)ZnO, (b) Fe_3O_4/ZnO/CuO (1:1:0.3), (c) Fe_3O_4/ZnO/CuO (1:1:0.5), (d) Fe_3O_4/ZnO/CuO (1:1:1), (e) Fe_3O_4/ZnO/CuO (1:1:3)

To investigate the various factors that affect the photocatalytic properties, the Fe_3O_4/ZnO/CuO nanocomposites with different molar ratios in MB solution were individually irradiated with UV and visible waves at 20-40-60-80-100-120 minutes. Fig. 8 shows the absorption spectrum of MB before photocatalytic activity. The absorption rate of methylene blue is approximately 1.067 at 665 nm. The reduction of this amount in the presence of Fe_3O_4/ZnO/CuO nanocomposite and ZnO samples under visible and UV radiation reflects the color of this industrial dye. It demonstrates the ability of this nanocomposite to treat industrial wastewater.

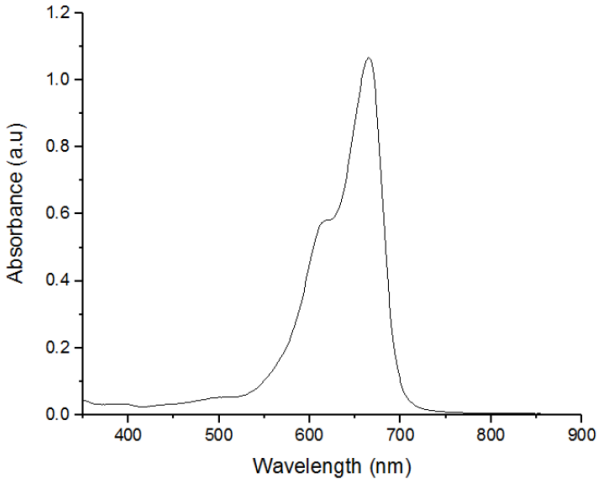

Fig. 8. Absorption spectrum of methylene blue before photocatalytic activity.

Fig. 9 shows the results of the photocatalytic activity under UV irradiation for over 120 minutes. The methylene blue absorption peak, which had an initial concentration of 0.005 g / L, decreased after 120 min in each sample. The amount of methylene blue dye removal by the Fe_3O_4/ZnO/CuO samples with a molar ratio of 1:1:0.5 is higher than in other samples. The photocatalytic activity of samples is 58.76%,65.32%,72.82%,49.39%, and 35.33% for ZnO, Fe_3O_4/ZnO/CuO with the molar ratio of 1:1:0.3,1:1:0.5,1:1:1,1:1:3 respectively, which were calculated using the formula.
Fig. 10 illustrates a comparative diagram of the photocatalytic performance of Fe_3O_4/ZnO/CuO nanocomposites with different amounts of CuO under UV irradiation for 20 to 120 minutes. Under UV irradiation, Fe_3O_4/ZnO/CuO nanocomposites with 1: 1: 1 and 1: 1: 3 molar ratios have lower photocatalytic activity than pure ZnO. The shift of the absorption edge towards the visible spectrum and the reduction in band gap of the nanocomposites can be attributed to the incorporation of CuO. Due to the differences between the UV wave energy with the amount of energy which was needed to transfer electrons from the valence band to the conduction band in Fe_3O_4/ZnO/CuO nanocomposites, and the low efficiency of electron-cavity generation compared to ZnO, the above nanocomposites exhibit less photocatalytic activity.

[DOI: 10.22068/ijmse.4019]

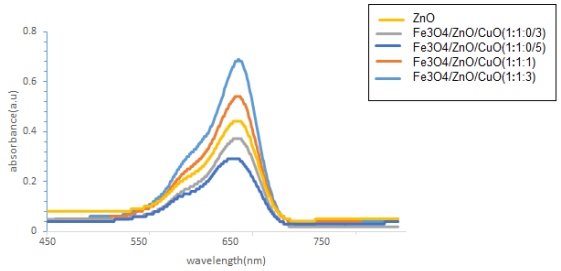

Fig. 9. Photocatalytic activity of Fe_3O_4/ZnO/CuO nanocomposites under UV radiation.

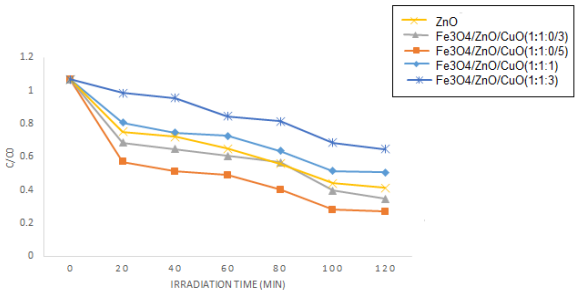

Fig. 10. Comparative diagram of Fe_3O_4/ZnO/CuO nanocomposites' photocatalytic efficiency under UV radiation.

Fig. 11 shows the results of the photocatalytic activity under visible irradiation for over 120 minutes. The Fe_3O_4/ZnO/CuO composite with a 1:1:0.5 molar ratio demonstrated superior methylene blue dye removal compared to other samples. The photocatalytic degradation efficiencies were measured at 48.45% for pure ZnO, and for Fe_3O_4/ZnO/CuO composites: 62.27% at 1:1:0.3 ratio, 88.7% at 1:1:0.5 ratio, 77.94% at 1:1:1 ratio, and 57.82% at 1:1:3 ratio. Fig. 12 shows a comparative diagram of the photocatalytic activity of Fe_3O_4/ZnO/CuO nanocomposites with different amounts of CuO under visible irradiation for 20 to 120 minutes. The Fe_3O_4/ZnO/CuO nanocomposite with a 1: 1: 0.5 molar ratio exhibits the best photocatalytic activity. However, the photocatalytic activity of the samples improved concerning pure ZnO, indicating the higher photocatalytic activity of Fe_3O_4/ZnO/CuO nanocomposites in the visible light range.

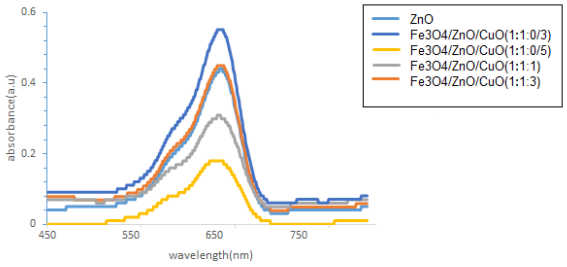

Fig. 11. photocatalytic activity of Fe_3O_4/ZnO/CuO nanocomposites under visible radiation.

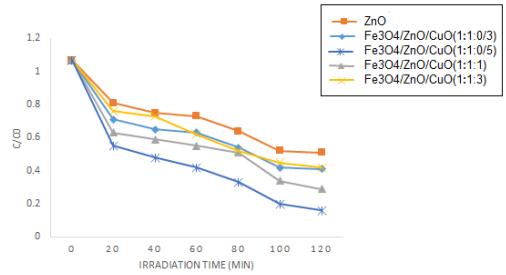

Fig. 12. Comparative diagram of photocatalytic efficiency of Fe_3O_4/ZnO/CuO nanocomposites under visible radiation.

To investigate the influence of ultrasound on the photocatalytic activity of the Fe_3O_4/ZnO/CuO nanocomposites with different molar ratios, the nanocomposites were irradiated with ultrasonic and visible light for 20-120 minutes in a methylene blue solution, and their photocatalytic activity was measured. Fig. 13 illustrates this. The results showed that the Fe_3O_4/ZnO/CuO nanocomposites with the molar ratio of 1:1:3 have the highest photocatalytic activity under ultrasound and visible light irradiation. The enhanced performance can be attributed to CuO's appropriate band gap characteristics. Under ultrasonic conditions, CuO showed higher activation compared to ZnO, and increasing the CuO content led to improved photocatalytic activity. As illustrated in Fig. 13, complete photocatalytic degradation (100% efficiency) was achieved after 120 minutes of treatment.

[DOI: 10.22068/ijmse.4019]

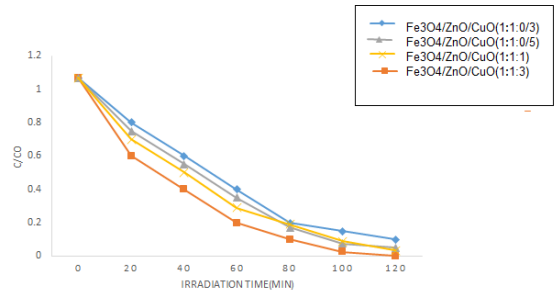

Fig. 13. Comparative diagram of photocatalytic efficiency of Fe_3O_4/ZnO/CuO nanocomposites under visible and ultrasound radiation.

The Fe_3O_4/ZnO/CuO nanocomposites with different molar ratios were investigated under UV, visible, and ultrasonic waves, and their comparative results are shown in Fig. 14. Enhancing photocatalytic activity of the nanocomposite under visible light and ultrasonic by increasing CuO content is mainly attributed to the narrow band gap of CuO, which enables strong visible-light absorption and promotes efficient charge separation through the formation of the n-p heterojunction. In this procedure, CuO acts as an effective electron trap, repressing recombination and enhancing the generation of reactive species. Under ultrasonic-visible light, the highest efficiency was observed, which can be driven by two reasons. Firstly, Ultrasonic increases the production of active radicals for photocatalytic activity, and also improves the organic transfer of color between the catalyst surface. secondly, the de-agglomeration of photocatalysis particles by ultrasonication leads to an increase in the specific surface area. The ultrasonic process operates through cavitation that forms holes, leading to elevated temperature and pressure conditions in the reaction medium. This process involves the formation, gradual growth, and eventual bursting of a series of bubbles by sonication. Under such conditions, hot spots are created that can convert water molecules into active hydroxyl radicals and hydrogen peroxide, and these active radicals destroy toxic compounds.

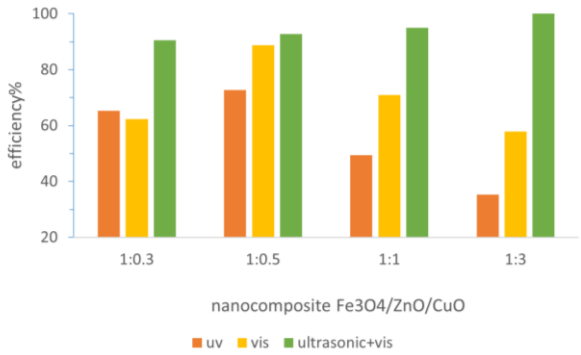

Fig. 14. Comparative diagram of photocatalytic efficiency of Fe_3O_4/ZnO/CuO nanocomposites under UV, visible, and ultrasonic radiation.

Based on other related researche, stability of the catalysts under light and ultrasonic irradiation was evaluated by the same batch of nanocomposites for four cycles, with the same amount of fresh MB solutions added after each run. The results in Fig. 15 show that the catalysts exhibit good stability and magnetic recyclability from the treated solutions after successive degradation reactions.
The XRD and FTIR measurements were also performed on the catalysts after multiple cycles, and compared with the results obtained before the reaction. In Fig. 15(a), all XRD peaks corresponding to cubic spinel, hexagonal wurtzite, and monoclinic structures remained at the same values after four cycles. So, there is no change in the crystalline structure.
The same conclusion is drawn from the IR absorption measurements because the IR peaks of the functional groups remain unchanged after photocatalytic degradation, Fig. 15(b) [30].

[DOI: 10.22068/ijmse.4019]

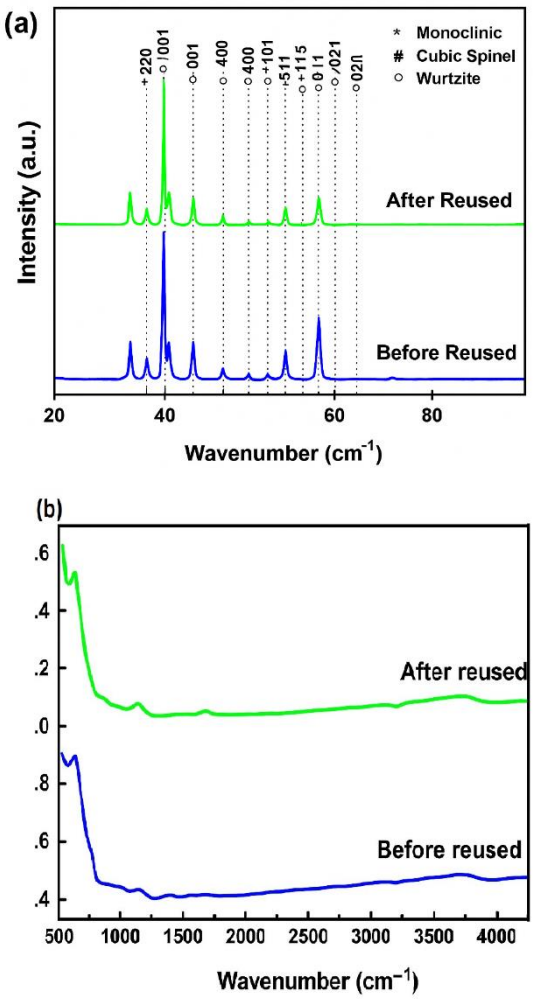

Fig. 15. a) XRD patterns of Fe_3O_4/ZnO/CuO nanocomposites after and before reussed,b) IR peaks of Fe_3O_4/ZnO/CuO nanocomposites after and before reussed [30]

Various factors such as the generation, trapping of electrons, charge carrier recombination, the average size of the crystals, and the energy of the band gap, are important factors that we can propose the mechanism of the photocatalyst. The varying molar proportions of CuO in the samples significantly influence the photocatalytic mechanism. Research has shown that a larger specific surface area creates more active surface sites, which reduces the interfacial charge carrier transfer resistance and enhances photocatalytic performance. The nanocomposites show different patterns of photocatalytic performance when exposed to visible light versus UV radiation.

The diffuse reflectance spectroscopy analysis revealed that ZnO has a band gap of 3.24 eV, while CuO exhibits a band gap of 1.54 eV[30]. As an n-type semiconductor, ZnO's electrons in the valence band become excited and move to the conduction band when exposed to UV radiation, which is possible due to its specific band gap energy. In contrast, CuO, being a p-type semiconductor, can achieve electron transfer from the valence to the conduction band through visible light exposure. The complementary band gap energies of ZnO, CuO, and Fe_3O_4 can enhance electron transfer between these materials. When exposed to visible light, CuO generates electron-hole pairs because of its favorable band gap. Additionally, electrons from ZnO's valence band, which possess lower energy compared to its conduction band, can move into structural defects like oxygen vacancies. When CuO's excited electrons migrate to ZnO's conduction band, they can interact with Fe^{3+} to form Fe^{2+} ions. These unstable Fe^{2+} ions then react with oxygen molecules to generate superoxide radicals. Simultaneously, holes created in ZnO's valence band can either transfer to CuO's valence band or interact with water molecules to create OH^-. Additionally, holes in CuO can also generate hydroxyl radicals through water interaction. Under UV light, the capture of electrons by Fe^{3+} ions enhances the probability of hole-mediated hydroxyl radical formation, which then breaks down organic pollutants. During this process, electrons from ZnO's valence band are exclusively excited to its conduction band, creating holes in the valence band. These excited electrons are captured by Fe^{3+} ions, forming Fe^{2+} ions that produce superoxide radicals. Concurrently, the photogenerated holes react with water molecules to form OH- radicals, which are the key agents in decomposing methylene blue during the catalytic reaction [26-28].

The mechanism behind MB degradation using ultrasonic treatment has been verified. When ultrasonic waves are applied, they induce acoustic cavitation, generating extreme conditions of temperature (5000 K) and pressure (1000 atm). This process produces light across a broad wavelength spectrum (sonoluminescence), activating both ZnO and

[DOI: 10.22068/ijmse.4019]

CuO semiconductors and forming electron-hole pairs [28]. These electron-hole pairs contribute to MB degradation through the same mechanisms observed in photocatalysis. When exposed to both visible light and ultrasound, CuO shows enhanced activation due to its suitable band gap energy. This explains why the nanocomposite containing the highest proportion of CuO (Fe_3O_4/ZnO/CuO in a 1:1:3 molar ratio) demonstrates superior photosonocatalytic performance under visible light conditions. Moreover, the extreme temperature and pressure conditions created by ultrasound in aqueous environments promote the direct formation of OH^- radicals through Fenton reactions [29]:

$$H_2O + \text{Ultrasound} \rightarrow OH^- + H^+ \quad \text{(Eq.5)}$$

$$H^+ + O_2 \rightarrow HO_2^- \quad \text{(Eq. 6)}$$

$$2HO_2^- \rightarrow H_2O_2 + O_2 \quad \text{(Eq. 7)}$$

$$2OH^- \rightarrow H_2O_2 \quad \text{(Eq. 8)}$$

According to Yuan and colleagues' research [30], the H_2O_2 produced (as shown in Eq. 7) can interact with Fe^{2+} to generate OH- radicals and Fe^{3+} ions. The increased production of OH radicals through various pathways under ultrasonic irradiation results in improved degradation efficiency.

The reason that the ternary nanocomposite with the ratio of 1:1:0.5 is optimal under visible light, while 1:1:3 is best under sonolysis, is attributed to the narrow band gap of CuO, which enables strong visible-light absorption and promotes efficient charge separation through the formation of the n-p heterojunction. In this procedure, CuO acts as an effective electron trap, repressing recombination and enhancing the generation of reactive species. In contrast, under UV irradiation, increasing the ratio of CuO in the nanocomposite reduces the photocatalytic performance because CuO does not absorb UV efficiently and partially covers the surface of the primary semiconductor (reducing the specific interface areas). Also, agglomeration occurs by increasing CuO content, which limits the UV absorption. Moreover, extra CuO can behave as recombination centers, accelerating electron–hole recombination and lowering the overall photocatalytic activity.

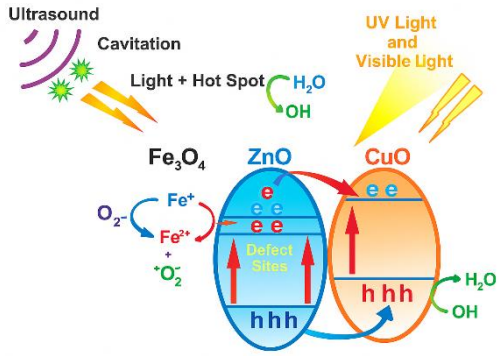

Fig. 16. Schematic of the photocatalytic mechanism of Fe_3O_4 / ZnO / CuO nanocomposites

4 Conclusions

In conclusion, the Fe_3O_4/ZnO/CuO nanocomposites were successfully produced using the sol-gel synthesis technique. The degradation of methylene blue was examined under both light and ultrasonic irradiation to analyse the photocatalytic activity. Results revealed that ultrasonic treatment played a crucial role and significantly improved the photocatalytic performance of the nanocomposite materials. The optimal composition of the photocatalyst nanocomposite material was investigated through structural characterization using various techniques. SEM images shown that the nanocomposite exhibited a cauliflower-like structure with particle size distribution ranging from 25.3 to 57.08 nm, as measured by ImageJ software. EDX analysis also confirmed improved dispersion of the samples. Additionally, dot mapping of the nanocomposite structure indicated that the elements were uniformly distributed throughout the material. Dynamic Light Scattering (DLS) results showed that increasing the copper oxide content in the Fe_3O_4/ZnO/CuO nanocomposite led to a reduction in particle size distribution.

[DOI: 10.22068/ijmse.4019]

Moreover, the addition of CuO decreased the band gap energy, shifting light absorption toward the visible region. The photocatalytic performance revealed 100% degradation of MB for Fe_3O_4/ZnO/CuO nanocomposite at a 1:1:3 molar ratio under ultrasound and visible light after 120 minutes. Additionally, the use of an external magnet allowed for easy separation and recovery of the nanocomposite from the solution after the reaction. These findings highlight the effectiveness of the ternary Fe_3O_4/ZnO/CuO nanocomposite catalyst in removing organic pollutants from wastewater.

Acknowledgements

The authors gratefully acknowledge the mechanical faculty of Tabriz University and the laboratory of the Materials Science and Engineering Department of Tabriz University.

Refrences

1. Zhu, L.; Zhou, Y.; Fei, L.; Cheng, X.; Zhu, X.; Deng, L.; Ma, X. "Z-scheme CuO/Fe_3O_4/GO heterojunction photocatalyst: Enhanced photocatalytic performance for elimination of tetracycline." *Chemosphere* 2022, *309* (Pt 2), 136721.
2. Alzuabidi, H. A.; Naghipour, A.; Fardood, S. T. "Green synthesis and characterization of $Cu_{0.5}Zn_{0.5}FeAlO_4$ magnetic nanoparticles with enhanced photocatalytic activity." *J. Ultrafine Grained Nanostruct. Mater.* 2024, 158–167.
3. Hu, Y.; Jensen, L.; Schatz, G. "Photocatalytic reaction pathways on TiO_2 surfaces: a theoretical study." *J. Am. Chem. Soc.* 2006, *128*, 15734–42.
4. Ge, M.; Cao, C.; Huang, J.; Li, S.; Chen, Z.; Zhang, K.; et al. "A review of one-dimensional TiO_2 nanostructured materials for environmental and energy applications." *Mater. Chem. A* 2016, *4*, 6772–6801.
5. Asghar, A.; Aziz, A.; Mohd, A. "Advanced oxidation processes for in situ production of hydrogen peroxide/hydroxyl radical for textile wastewater treatment: a review." *J. Cleaner Prod.* 2015, *87*, 826–38.
6. Shakir, A. K.; Ghanbari-Adivi, E.; Baron, A. S.; Soltani, M. "Investigation of the Effect of Calcination Time on the Antibacterial, Antifungal and Anticancer Activities of TiO_2/ZnO Nanocomposites." Iran. J. Mater. Sci. Eng. 2025, 22 (1).
7. Safavi, M. S.; Bozorg, S.; Ahadzadeh, I.; Safavi, M. S. "Development of heterogeneous nano-zeolite catalyzing Fenton-like oxidation processes for metalworking fluid wastewater treatment: A comparison with conventional methods." *J. Ultrafine Grained Nanostruct. Mater.* 2024, 190–202.
8. Asai, M. M.; Tapadia, K. "Biofabricated magnetic CuO@Fe_3O_4 nanocomposites: Synthesis, characterization and Brilliant Green dye removal from aqueous media and its kinetics study." *J. Indian Chem. Soc.* 2025, *102* (5), 10166.
9. Ajmal, A.; Majeed, I.; Malik, R.; Idriss, H.; Nadeem, M. "Principles and mechanisms of photocatalytic dye degradation on TiO_2-based photocatalysts: a comparative overview." *RSC Adv.* 2014, *4*, 37003–26.
10. Soleimani-Amiri, S.; Hossaini, Z.; Azizi, Z. "Synthesis and investigation of biological activity of new oxazinoazepines: Application of Fe_3O_4/CuO/ZnO@MWCNT magnetic nanocomposite in reduction of 4-

[DOI: 10.22068/ijmse.4019]

nitrophenol in water." *Polycycl. Aromat. Compd.* 2023, *43* (4), 2938–59.

11. Cruz, M.; Gomez, C.; Duran-Valle, C.; Pastrana-Martinez, L.; Faria, J.; Silva, A.; et al. "Bare TiO_2 and graphene oxide TiO_2 photocatalysts on the degradation of selected pesticides and influence of the water matrix." *Appl. Surf. Sci.* 2015, *268*, 1–9.
12. Rahmat, R.; Heryanto, H.; Ilyas, S.; Fahri, A. N.; Mutmainna, I.; Rahmi, M. H.; Tahir, D. "The relation between structural, optical, and electronic properties of composite CuO/ZnO in supporting photocatalytic performance." *Desalination Water Treat.* 2022, *270*, 289–301.
13. Shen, Y.; Wang, Y.; Chen, Y.; Park, J. K.; Fang, S.; Feng, K. "Synthesis of Fe_3O_4/CuO/ZnO/RGO and its catalytic degradation of dye wastewater using dielectric barrier discharge plasma." *Arab. J. Chem.* 2023, *16* (4), 104571.
14. Ohtani, B. "Photocatalysis A to Z – What we know and what we do not know in a scientific sense." *J. Photochem. Photobiol. C* 2008, *11*, 157–78.
15. Rashid, H.; Muhammad, E.; Hassan, M.; Rauf, A.; Bashir, A.; Ali, W.; et al. "Synthesis, structural and photocatalytic properties of ZnO-CuO, ZnO-Graphene and ZnO-CuO-Graphene nanocomposites." *Polyhedron* 2025, *273*, 117471.
16. Li, X.; Liu, J.; Liu, E.; Wan, J.; Bai, Z. "A review of heterogeneous photocatalysts for environmental remediation: materials and processes." *Chemosphere* 2016, *172*, 124–40.
17. Takahashi, M.; Okada, K.; Malfatti, L.; Innocenzi, P. "Formation of interfaces responsive and adaptive to environment via the sol-gel method." *J. Sol-Gel Sci. Technol.* 2024, *112* (1), 174–81.
18. Malhotra, A.; Saini, A.; Jindal, N.; Kumar, R. "Combustion synthesized Fe_3O_4/α-Fe_2O_3/C nanocomposites for efficient radiative and non-radiative degradation of methylene blue dye." *Inorg. Chem. Commun.* 2025, *173*, 113808.
19. Bopape, D. A.; Hintsho-Mbita, N. C. "Commelina benghalensis-mediated CuO–ZnO nanocomposite: Effect of the pn heterojunction on the photocatalytic activity against Congo red and carbamazepine." *Inorg. Chem. Commun.* 2025, *154*, 114529.
20. Intharaksa, O.; Nanan, S.; Patdhanagul, N.; Panphojan, T.; Srikakul, T.; Tantisuwichwong, N.; et al. "Preparation of magnetic CuO/Fe_3O_4/ZnO photocatalyst for complete degradation of methylene blue under natural sunlight irradiation." *J. Phys. Chem. Solids* 2023, *182*, 111577.
21. Melese, A.; Wubet, W.; Abebe, A.; Hussen, A. "A comprehensive review on recent progress in synthesis methods of ZnO/CuO nanocomposites and their biological and photocatalytic applications." *Results Chem.* 2025, *7*, 102141.
22. Wahba, M. A.; Yakout, S. M. "Microwave-synthesized ZrO_2/ZnO heterostructures: fast and high charge separation solar catalysts for dyes-waste degradation." *J. Sol-Gel Sci. Technol.* 2022, *104* (2), 330–41.
23. Ross, J. R. H. "Catalyst characterization." In *Contemporary Catalysis Fundamentals and Current*

[DOI: 10.22068/ijmse.4019]

Applications; 2019; Chapter 5, pp 121–132.

24. Chen, X.; Selloni, A. "Introduction: Titanium dioxide (TiO_2) nanomaterials." *Chem. Rev.* 2014, *114*, 9281–82.
25. Etay, H.; Kumar, A.; Yadav, O. P. "Kinetics of photocatalytic degradation of methylene blue dye in aqueous medium using ZnO nanoparticles under UV radiation." *J. Anal. Pharm. Res.* 2023, *12* (1).
26. Asli, S. A.; Taghizadeh, M. "Sonophotocatalytic degradation of pollutants by ZnO-based catalysts: A review." *Chem. Select* 2020, 13720–73.
27. Benamara, M.; Nassar, K. I.; Essid, M.; Frick, S.; Rugmini, R.; Sekhar, K. C.; Silva, J. P. "Visible light-driven removal of Rhodamine B using indium-doped zinc oxide prepared by sol–gel method." *J. Sol-Gel Sci. Technol.* 2024, *111* (2), 553–65.
28. Yuan, N.; Zhang, G.; Guo, S.; Wan, Z. "Enhanced ultrasound-assisted degradation of methyl orange and metronidazole by rectorite-supported nanoscale zero-valent iron." *Ultrason. Sonochem.* 2016, *28*, 62.
29. Khan, M. A. N.; Siddique, M.; Wahid, F.; Khan, R. "Removal of reactive blue 19 dye by sono, photo and sonophotocatalytic oxidation using visible light." *Ultrason. Sonochem.* 2015, *26*, 370–77.
30. Taufik, A.; Saleh, R. "Synthesis of iron (II, III) oxide/zinc oxide/copper (II) oxide(Fe_3O_4/ZnO/CuO) nanocomposites and their photosonocatalytic property for organic dye removal." *J. Colloid Interface Sci.* 2017, *491*, 27–36.

[DOI: 10.22068/ijmse.4019]